NASA TECHNICAL MEMORANDUM

NASA TM-73804

NASA TM-73804

PERFORMANCE OF THE 12 GHz, 200 WATT TRANSMITTER EXPERIMENT PACKAGE FOR THE HERMES SATELLITE

by Robert E. Alexovich
Lewis Research Center
Cleveland, Ohio 44135

TECHNICAL PAPER to be presented at the
Symposium on "Hermes (Communications Technology Satellite): Its Performance and Applications" sponsored by
The Royal Society of Canada in cooperation with
the Canadian Department of Communications and
the National Aeronautics and Space Administration, USA
Ottawa, Ontario, November 29 - December 1, 1977

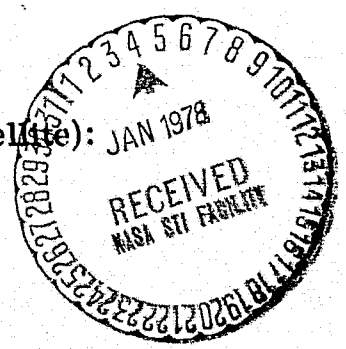

PERFORMANCE OF THE 12 GHz, 200 WATT TRANSMITTER EXPERIMENT PACKAGE FOR THE HERMES SATELLITE

ROBERT E. ALEXOVICH

National Aeronautics and Space Administration
Lewis Research Center
Cleveland, Ohio 44135

E-9385

SUMMARY

Performance characteristics from on-orbit tests of the Transmitter Experiment Package (TEP) for the Hermes Satellite are presented. The tests were conducted from February 8, 1976 through August 8, 1977.

The TEP consists of a Power Processing System (PPS), an Output Stage Tube (OST) and a Variable Conductance Heat Pipe System (VCHPS), all of which are described. The OST is a coupled-cavity Traveling Wave Tube (TWT) with a Multistage Depressed Collector (MDC) and a stepped velocity-tapered slow wave structure for efficiency enhancement. It has an rf output power of 233 watts and overall efficiency of 50.75 percent at a center band frequency of 12.080 GHz. The PPS provides the required operating voltages, regulation, control and protection for the OST. The VCHPS consists of a fin radiator and three dual-artery stainless steel heat pipes using methanol and a mixture of inert gases. Test results presented include efficiencies, rf output power and body current. A discussion of thermal anomalies which occurred is presented.

INTRODUCTION

The Hermes Satellite was developed in a joint U.S. - Canadian program by NASA and the Canadian Department of Communications. One of the major responsibilities of the United States in the joint program was to provide a 200 watt, 12 GHz, 50 percent efficient high power transmitter for the spacecraft.

Before the Hermes Satellite, microwave amplifiers for space applications were limited to frequencies below 8 GHz, power levels of 50 watts and efficiencies of 10 to 25 percent. These relatively low efficiencies represent an unnecessary waste of power which results in increased satellite weight and cost and a reduction in reliability; the latter being the result of excessive waste heat.

The key to future uses of higher rf powers for communications satellite applications is the development of high power microwave amplifiers with high efficiency. As rf power output increases, the importance of high efficiency is emphasized. For high power satellites, the efficiency of the transmitter is a major factor in determining the size of the solar array, the complexity and size of the thermal control system, and the weight of the power processing system for the transmitter output amplifier. With the launching of the Hermes Satellite, the era of high power (200W) and high efficiency (50 percent) space amplifiers has begun.

The Transmitter Experiment Package (TEP) for the Hermes Satellite has a measured rf output of 233 watts and an overall efficiency of 50.75

percent at a center band frequency of 12.080 GHz. The operating bandwidth of the TEP is 85 MHz. It consists of the Output Stage Tube (OST), the Power Processing System (PPS) and the Variable Conductance Heat Pipe System (VCHPS). It is an experiment aboard the Hermes Satellite that was launched on January 17, 1976 at 23:27:54 GMT.

The principal technological objectives of the TEP development are:

1. To demonstrate in space an amplifier operating with an efficiency $\geq$ 40 percent and a saturated rf output power $\geq$ 180 watts at a frequency of 12 GHz.
2. To demonstrate reliable high-efficiency performance for a transmitter experiment package for two years in a space environment.
3. To obtain fundamental data for further advancement in the state-of-the-art of high power microwave amplifier operations in space.

This paper presents a description of the TEP, its unique design characteristics, and a summary of the on-orbit evaluation of the TEP performance.

TRANSMITTER EXPERIMENT PACKAGE

The TEP is used as an output power amplifier in the Hermes spacecraft transponder (fig. 1) to amplify signals in the RB1/TB1 signal path. The communications requirements of the TEP are given in table I. The TEP consists of a nominal 200 watt Output Stage Tube (OST), a supporting Power Processing System (PPS), and a Variable Conductance Heat Pipe System (VCHPS).

The TEP is mounted within the spacecraft on the south panel as shown in figure 2. The OST is mounted on the evaporater saddle of the VCHPS which in turn is mounted on the PPS baseplate; this whole assembly is then mounted on the spacecraft south panel. The OST is located such that the multistage depressed collector enclosure protrudes through the aft section of the spacecraft for direct thermal radiation from the collector enclosure.

Output Stage Tube

The OST[1] is a coupled-cavity Traveling Wave Tube (TWT) augmented with a Multistage Depressed Collector (MDC) as shown schematically in figure 3. This class of linear beam microwave amplifiers converts the kinetic energy of an electron beam into rf energy.

An electron beam is formed by convergent optics in the electron gun. Electrons, emitted by a thermionic cathode, are accelerated to approximately 1/5 the speed of light by the potential difference between the cathode and the anode. The cathode and anode voltages with respect to the TWT body are -11,200 volts and 250 volts respectively. The electrons pass through an interaction region of the TWT located between the input and output waveguides. This region of the TWT is composed of cylindrical cavities, coupled to form a lumped element transmission line or slow wave structure. It contains three line sections separated by terminations (or severs). Beam focusing is accomplished by magnets placed outside of the cavity structure along the transmission line. The rf wave, in the transmission line, interacts with the electron beam as it passes through each cavity. The kinetic

energy of the electron beam is coverted to rf energy by fringing rf fields in each cavity which interact with the electron beam.

The output section utilizes cavities with physical dimensions designed to reduce the velocity of the rf wave in the transmission line. The velocity reduction is done in two steps to maintain synchronism between the rf wave and the electron beam as the electron velocities are reduced. This velocity tapering of the output section produces an interaction efficiency of 26 percent. As the beam exits from the coupled-cavity region of the TWT, it enters the MDC. Magnetic refocusing of the electron beam[2] (see fig. 3) establishes the desired electron entry conditions into the MDC.

The MDC[3] is used to convert kinetic energy remaining in the electron beam to potential energy and thereby reduce the power required to operate the TWT. The MDC is composed of ten collector electrodes or plates. Each, with the exception of the tenth collector, has a centrally-located hole which allows the electron beam to penetrate the collector region. The tenth collector has a centrally located spike as shown in figure 3. The depth of penetration of an electron is determined by its entry velocity or remaining kinetic energy. Electrons are collected by the plates based on their kinetic energies. High energy electrons are collected by the tenth and its neighboring plates, while low energy electrons are collected by the first and its neighboring plates. The shapes of the collector electrodes are designed to produce equipotential surfaces and an electric field configuration necessary to sort and collect electrons in accordance with their entry

velocities. The electrons, therefore, are collected near the apex of their trajectories where they have near-zero velocity. In this manner, the electron kinetic energy is converted to potential energy and returned to the PPS. This reduces the power required to operate the OST. The tenth collector is connected to cathode potential; the collector electrodes from the tenth through the second are connected to descending voltages, each differing from its neighboring electrode by 1/10 of the cathode voltage. The use of the MDC results in reduced input power, and therefore, increased efficiency for all rf output powers up to and including saturation.

Heat produced in the MDC due to residual velocities of the collected electrons is radiated to the collector enclosure and in turn radiated to space. A combination of internal heat shields and a bellows-type external heat choke is used to reduce the heat flow back to the interaction section of the TWT. The packaged OST is shown in figure 4.

Power Processing System

Electrical power for operation of the TEP is delivered to the PPS at nominal supply voltages of 76 VDC and 27.5 VDC, respectively. The PPS[4] performs the following functions for TEP operations:

1. Develops proper operating voltages for the TWT and MDC.
2. Regulates supply voltages.
3. Provides fault sensing and protection.
4. Provides command control and sequencing for remote operation.

The electrical interface between the PPS and the OST and the space-

craft electrical systems is shown in figure 5. The collector and body currents are a function of rf output power and frequency. The values given are typical of center band saturated output operation. The sum of body and collector currents is constant and equal to the cathode current, 76 mA, for all operating conditions. Separate inverters are used for the cathode-collector, anode, and cathode heater supplies.

A simplified schematic of the basic PPS cathode-collector supply which supplies the main operating power for the OST, is shown in figure 6. This supply provides high-voltage power for operation of the OST. Input power from the 76V bus passes through an input filter and chopper pre-regulator. This power is converted to high voltage DC by a transistor chopper converter and high voltage transformer. There are multiple secondary windings each connected to a bridge rectifier as shown. The DC output of the bridge rectifiers are series connected to provide-11.2KV cathode supply and intermediate voltages for the MDC electrodes. Only the sum of these voltages or the cathode voltage is regulated. It is measured and compared to a reference. The resulting error is used to control the input pre-regulator. The switching frequency of the inverter is 10KHz. An active AC filter is used in the cathode voltage supply to meet minimum ripple requirements without exceeding stored energy limits that would be damaging to internal OST structure during internal arcs.

An exploded schematic of the PPS package is shown in figure 7. The package has outgassing vents in the top cover and side as shown and

the high voltage and low voltage sections are separated within the package. Heat developed within the PPS is conducted to the TEP baseplate and to the south panel.

Variable Conductance Heat Pipe System

The VCHPS[5] is used to remove heat from the TWT body and maintain controlled operating temperatures for all operating and non-operating levels of OST and for the range of solar thermal input encountered.

The VCHPS (fig. 8) consists of the heat pipe evaporator saddle, three variable conductance gas-loaded heat pipes, radiator and support structure. The radiator is held at three attachment points to the spacecraft and by four struts as shown. The plane of the radiator is parallel to the orbit plane.

The internal structure of heat pipes is shown in figures 9 and 10. The pipes consist of 0.50 inch O.D. stainless steel tubes with a 0.028 inch wall. The tube is internally threaded with 100 threads per inch. There is a stainless steel felt wick .020 inches thick, across the inner diameter, with stainless steel arteries, .063 inches I.D. attached as shown. Under normal operation at saturated power 90 percent of the heat transfer liquid is carried by the arteries. Priming foils, attached to the artery wick assembly as shown in figure 10 and located in the evaporator end of pipes are used to preclude blocking of the arteries by entrapped gas. The priming foils are stainless steel, 0.005 inch thick, with 0.010 inch diameter holes. The heat pipe saddle is made of

aluminum and soldered to the pipes.

The variable conductance heat pipes are filled with methanol as a working fluid and a mixture of 90 percent nitrogen and 10 percent helium as a control gas. The gas load in each pipe is adjusted such that the individual heat pipes become active at different levels of pipe temperature. The expected performance of the VCHPS is given in figure 11. For steady state operation at saturation, the heat rejection from the body of the OST is 155 watts. This produces an expected saddle temperature of approximately 37°C at equinox. The saddle temperature increases with increasing Sun illumination of the radiator.

DISCUSSION OF RESULTS

DC and RF Performance of the TEP

The results presented in this paper include test results from the period of June 14, 1976 through August 8, 1977. As of August 8, 1977, the TEP had been operated for a total of 8830 hours. The results obtained from tests during this period are compared to initial test results from February 8 through June 13, 1976[6]. It should be noted that included in these results are results of the first TEP operation during the season of eclipse by the Earth. The TEP was not operated during prior eclipse seasons due to a failure in the spacecraft power subsystem.

A series of tests were conducted to determine on-orbit communications, electrical and thermal performance of the TEP. Losses attendant to the large power consumption of the TEP necessitated special care to accommodate widely varying heat rejection rates from both the OST body and the MDC enclosure. Because the TEP thermal condition is influenced greatly by

its operating point, it was necessary to operate at constant rf power levels for periods up to two hours to achieve thermal equilibrium. This was done to establish repeatable test conditions. All tests were conducted using the CTS ground station facility at Lewis Research Center for uplink test signal transmission and downlink reception.

Some of the observed TEP performance characteristics are summarized in Table II. Average results obtained from prior testing are also presented for comparison.[6] Average OST rf output at saturation for the days of TEP operations are shown in figure 12. Due to erratic behavior of the rf output sensor at high temperatures, which occurs frequently at high power levels, no data is available from this source after day 300 for saturated power at center band (CB,12.080 GHz) frequency. For upper band edge (UBE, 12.123 GHz) and lower band edge (LBE, 12.038GHz) frequencies and for reduced powers at CB, the sensor response is normal. The average saturated CB rf output power for this period of operation is 233.4 watts. The OST saturated rf output powers are 151.4 and 185.5 watts at UBE and LBE respectively. The saturated rf output compares well with measured values for the first 90 days of operation, the difference between CB rf output at saturation being within the deviation for the two periods of measurement.

The measured efficiencies for saturated output is shown in figure 13. These results are compared in table II to corresponding measured efficiencies from the first 90 days of operation. Again the comparison shows that there has been no measurable change in performance with time. With the failure of the output power sensor at high temperatures no data is available for CB saturated power output. However, the energy

recovery of the MDC is sensitive to spent beam characteristics. As a result, an indication of rf output power extracted from the electron beam can be derived from the MDC electron velocity distributions and OST DC input power. Based on the constancy of OST DC input power, figure 14, and collector current distributions, it is concluded that saturated rf output power has not changed in the time period after day 70, 1977.

The OST beam focusing utilizes Samarium Cobalt permanent magnets. Stability of the focusing field distribution can be derived from observing beam interception or body current. Body current for 100 watts and saturated rf output power at CB, and for zero rf or DC operation is given in figure 15. A comparison of body current to values obtained from earlier test results, table II, shows that there has been no measurable effect due to environment or thermal cycling due to 8,830 hours of operation.

The cathode heater supply is current regulated and provides constant heater power, and both cathode and anode voltage are regulated and continuously monitored. The change in beam current, figure 16, is due to a change in emission from the cathode. This drop in beam current is well within design limits necessary to achieve two years of operating life. The expected effects of this reduction in beam current on DC input power, rf output power and body current are too small to be observable. It is expected that two years operating life (18,000 hours) will be achieved without significant degradation in performance.

OST Thermal Anomaly

On day 75, March 16, 1977, at 19:25 GMT, the OST body temperature in the region of the rf output unexpectedly began to increase. Figure 17 shows body time-temperature-profile on day 75 during the anomaly period. At 340 minutes, the body temperature increased from its normal operating temperature of 56°C, to 75°C at 377 minutes. At this time rf output power was reduced and body temperature was reduced. Figure 18 shows the OST DC input power history for the same period on day 75. It can be seen that from 250 minutes, when rf power was reduced, the input power was essentially constant. RF output power during this time was also constant, therefore, internal losses resulting in waste heat rejected by the TEP thermal control system were also constant. Changes in input or output power, failure in measurement, and Sun illumination were readily discounted as possible causes for the thermal anomaly. It was concluded that the anomalous increase in OST body temperature was caused by a change in:

1. Thermal conducting paths of the OST or
2. Performance of the VCHPS.

As of August 8, 1977, there have been three anomalies, day 75, day 82, and day 101. Figure 19 shows the Sun angles and eclipse durations for the anomaly days. All three days occurred during the eclipse season and during the period of near zero or positive Sun angles. Figure 20 shows the orbital position of the spacecraft at the time of each anomaly. The orientation of the spacecraft at the time of all the anomalies were such that the heat pipe radiator and gas reservoirs

are shadowed by the spacecraft, (see also figure 8). The resultant shadowing causes this region of the radiator to fall in temperature to near the freezing point of methanol, (-98°C) see figures 21 and 22. These sensor locations are shown in figure 8.

The thermal conducting path for removal of body loss heat is shown in figure 23. The OST is supported by an input and output saddle. The larger saddle is located at the output end because skin effect and beam interception losses are largest in this region of the body. The saddles are mounted on the OST baseplate which then is mounted on the heat pipe saddle. The whole assembly is then mounted on the PPS baseplate and the south panel of the spacecraft. The temperature sensors indicating abnormally high during each anomaly are located in the region of the OST output port. A section through AA of figure 23 is given in figure 24. Figure 24 shows the conducting paths from the OST body to the heat pipe saddle and spacecraft south panel. Indium foil shims are used in the thermal interfaces between the copper bus to the aluminum saddle, and aluminum saddle to OST baseplate. The remaining interfaces use RTV silicone elastomer as shown.

A detailed analysis of data from the anomalies has revealed the following:

1. The turn-on signature as indicated by the adiabatic temperatures of heat pipes 1, 2, and 3, shown in figures 25, 26, and 27 respectively, are normal. They turn on in sequence and their initial steady state temperatures are normal.

2. The difference between heat pipe 3 and heat pipe 1 adiabatic

temperatures, figure 28, prior to the anomaly and during the anomaly exceeds the normal difference by 1 to 2°C.

3. The signature of the anomalies, (see figure 29) for day 75, are characterized by a sudden drop to a low value of heat rejection (Point A), as exponential recovery (A-B) to a constant rate of heat removal depicted by the straight line section of the temperature rise (B-C). The constant value determined by this linear rise in all anomalies was 104 to 109 watts.

4. The thermal system recovers completely, without any measurable change, after each anomaly.

Based on ground tests with the VCHPS, it has been found that the abnormal difference between the adiabatic section temperatures of heat pipe 3 and heat pipe 1 can be duplicated by heat pipe depriming.

CONCLUDING REMARKS

On orbit tests were conducted to evaluate the performance of the Hermes transmitter experiment package. The OST efficiency at center band frequency and saturated output power was determined to be 50.75 percent. Corresponding rf output and OST DC input powers were 233.4 watts and 463.9 watts respectively. There were no observable degradations in TEP performance due to launch, pre-injection, and operating environments, nor were there observable degradations from operating for 8830 hours during 568 days in orbit.

The anomalous thermal behavior has not resulted in irreversable or permanent change in TEP performance. As of August 8, 1977, it has

been determined that the thermal anomalies are due to:

1. Depriming of the VCHPS resulting from unknown causes, or

2. Recoverable changes in OST-VCHPS thermal interfaces.

It is concluded that:

1. There are no observable degradations in TEP electrical performance due to launch, pre-injection and operating environment.

2. The most probable cause of anomalous thermal behavior has not resulted in irreversable or permanent change in TEP performance.

3. It is expected that two years of operating life (18,000 hours) will be achieved without significant degradation in performance.

REFERENCES

1. H. G. Kosmahl, B. D. McNary, and O. Sauseng, "High-Efficiency, 200 Watt, 12-Gigahertz Traveling Wave Tube," NASA TN D-7709, 1974.

2. H. G. Kosmahl, "Electron Beam Controller," U.S. Patent 3,764,850, 1973.

3. H. G. Kosmahl, "A Novel Axisymmetric Electrostatic Collector for Linear Beam Microwave Tubes," NASA TN D-6093, 1971.

4. B. F. Farber, A. D. Schoenfeld and P. A. Thollot, "Power Processing System for a 200 W Communication Satellite Transmitter," in IEEE International Conference on Satellite Communications Systems Technology, Inst. Electr. Electron. Eng., 1975.

5. B. F. Farber, D. S. Goldin, B. Marcus and P. Mock, "Transmitter Experiment Package for the Communications Technology Satellite," TRW Defense and Space Systems Group, Contract NAS 3-15839, NASA CR-135035, 1977.

6. R. E. Alexovich, et al., "Early Performance of the 12-GHz 200-Watt Transmitter Experiment Package in the Communications Technology Satellite," NASA TM X-3555, 1977.

TABLE I

TEP COMMUNICATIONS REQUIREMENTS

Minimum Output Power (Average Across Band), Watts	180
Efficiency Goal, Percent	50
Gain, Saturated, dB	30 +2-1
Band Width, GHz	12.038 - 12.123
Differential Gain, dB	$\pm$ 1.5
Maximum Gain Ripple, dB Peak to Peak	5
Maximum Group Delay, Nanoseconds Peak to Peak	8
Noise Figure, dB	40
Maximum Load, VSWR	1.25
Design Life, Years	2

TABLE II

OBSERVED TEP PERFORMANCE CHARACTERISTICS

	February 8 - June 13, 1976 Average	St'd. Dev.	June 13, 1976 August 8, 1977 Average	St'd. Dev.
SATURATED EFFICIENCY, PERCENT				
CB (Center band freq., 12.080 GHz)	51.52	1.85	50.75	1.75
UBE (Upper band edge freq., 12.123 GHz)	37.0	1.22	37.80	3.34
LBE (Lower band edge freq., 12.038 GHz)	38.5	1.22	38.14	1.01
SATURATED RF OUTPUT, WATTS				
CB	241.1	8.68	233.4	7.26
UBE	151.3	6.96	151.4	11.51
LBE	185.7	5.76	185.5	1.09
SATURATED OST DC POWER, WATTS				
CB	469.9	6.6	463.9	8.12
UBE	406.1	5.7	401.9	1.81
LBE	482.6	8.8	475.3	9.46
BODY CURRENT, mA				
CB, SATURATED	6.43	0.27	6.32	0.34
CB, 100W	2.37	0.15	2.56	0.11
DC	1.64	0.10	1.62	0.05
BEAM CURRENT, mA	76.35	--	76.2	--

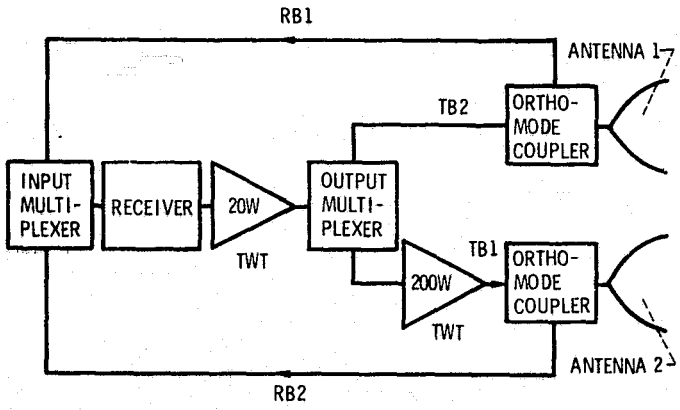

Figure 1. - Simplified diagram of the Hermes spacecraft transponder.

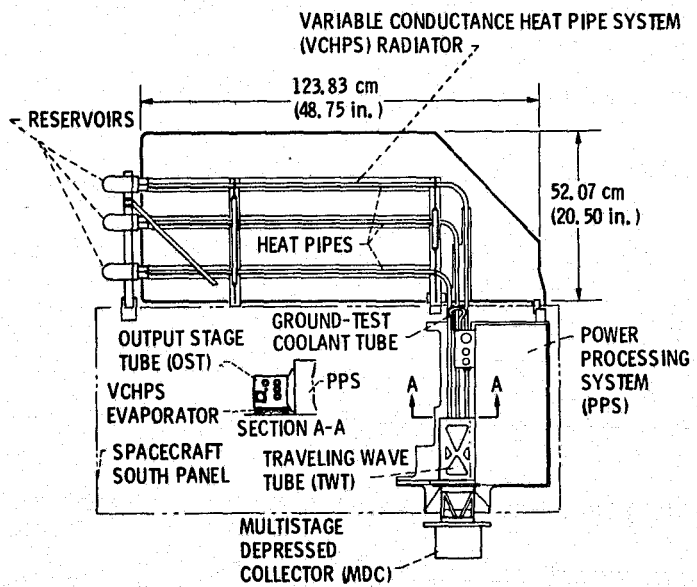

Figure 2. - Hermes transmitter experiment package.

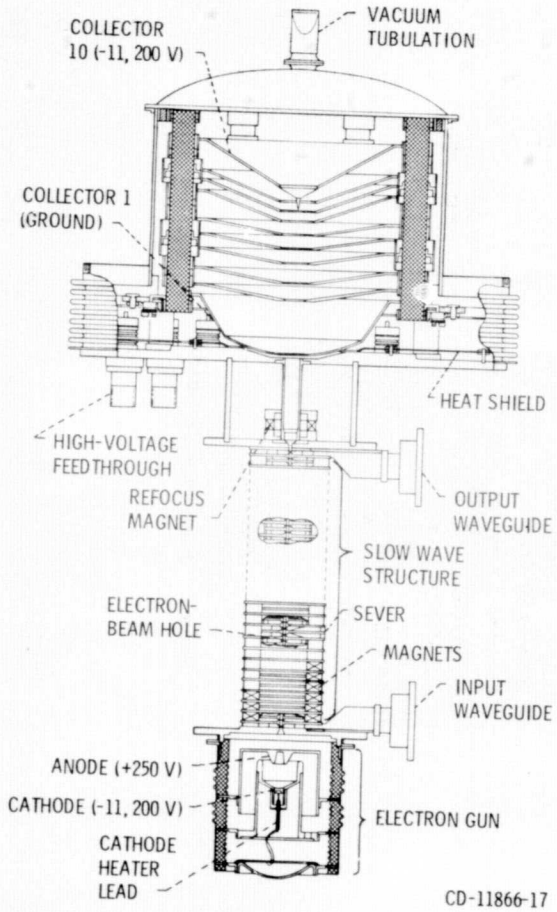

Figure 3. - Hermes traveling wave tube with multistage depressed collector.

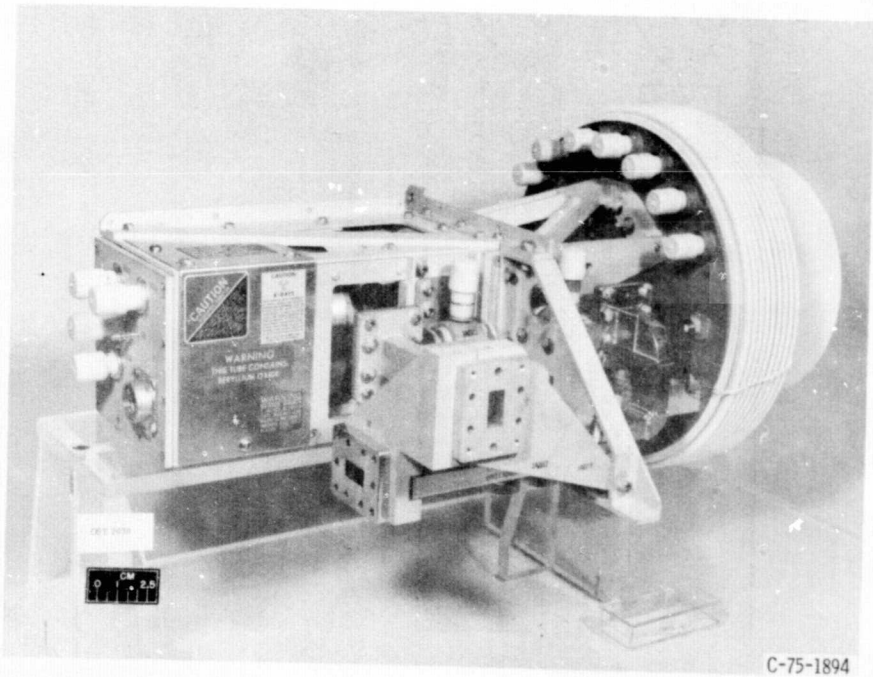

Figure 4. - Hermes output stage tube.

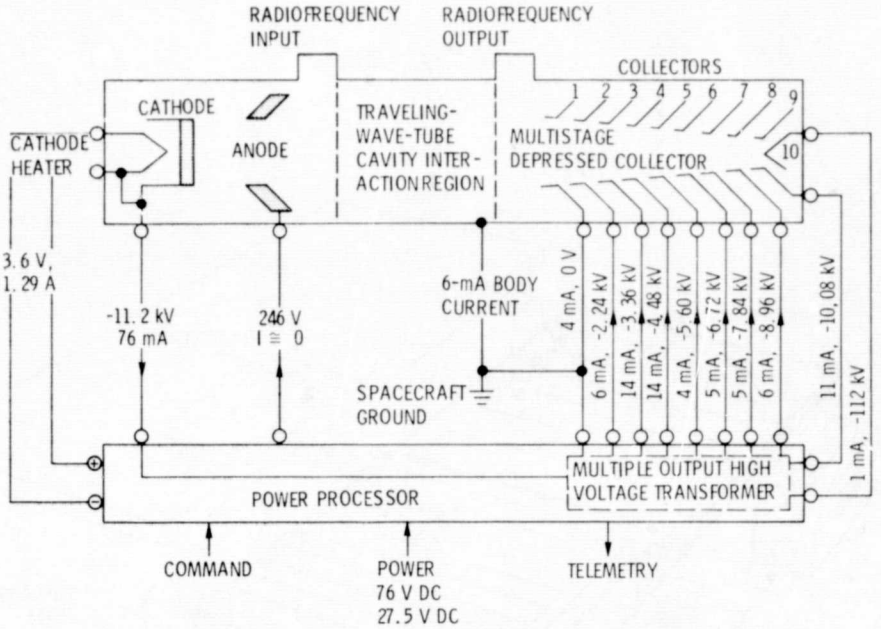

Figure 5. - Power interface between output stage tube and power processing system. (All voltages are with respect to spacecraft ground. Collector currents are typical of operation at center band, saturated.)

E-9385

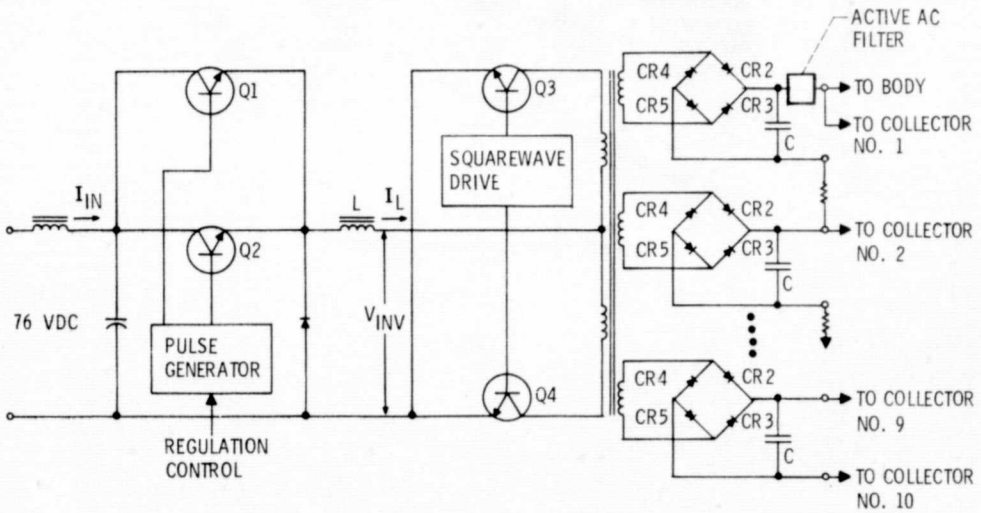

Figure 6. - Current source chopper preregulator/squarewave inverter used for collector, cathode supply.

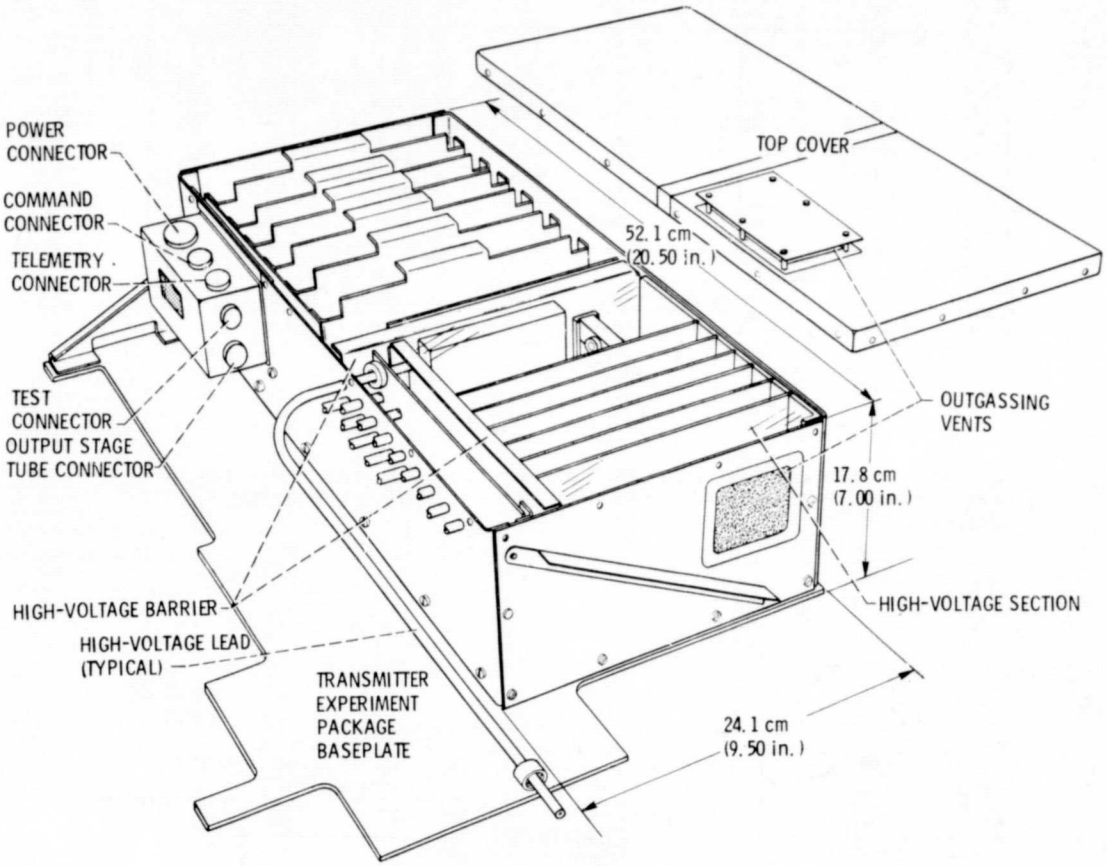

Figure 7. - Power processing system.

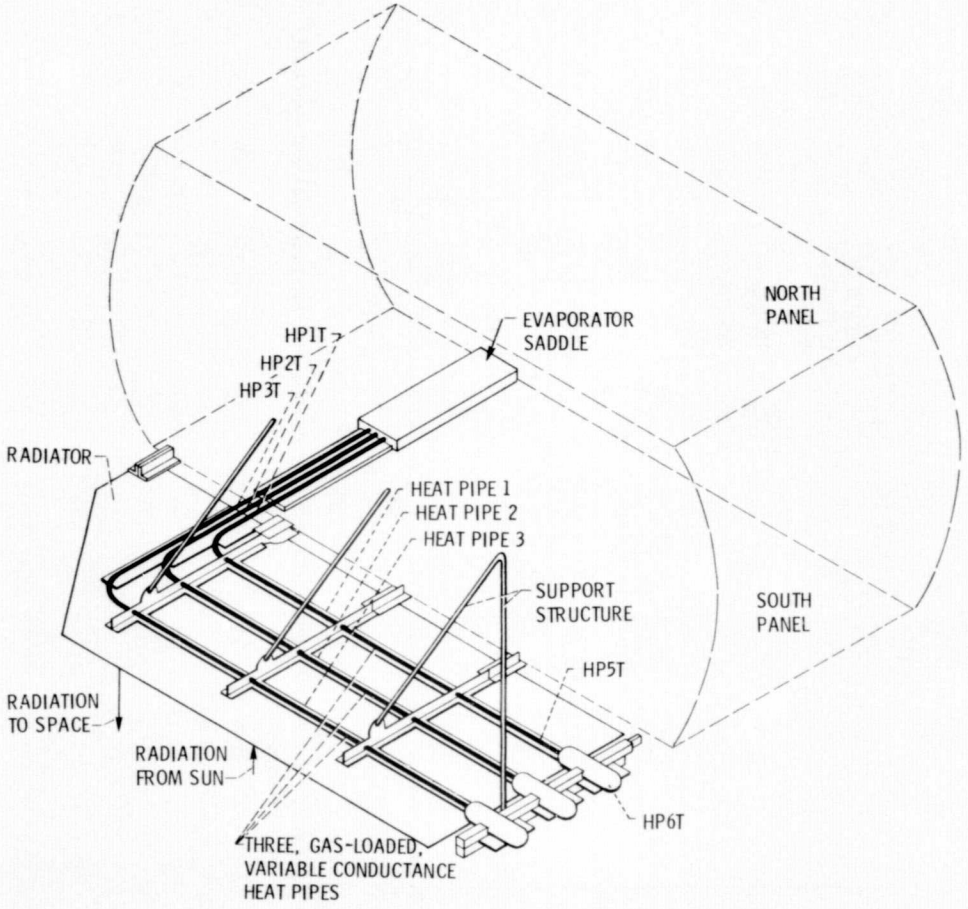

Figure 8. - Variable conductance heat pipe system.

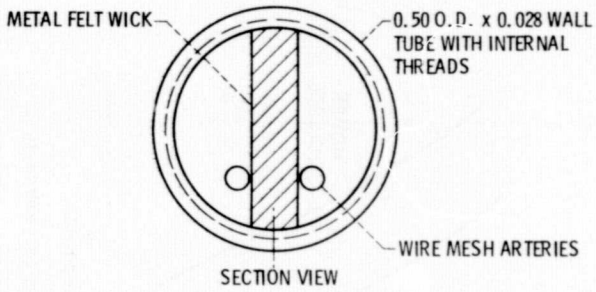

Figure 9. - TEP heat pipe wick configuration.

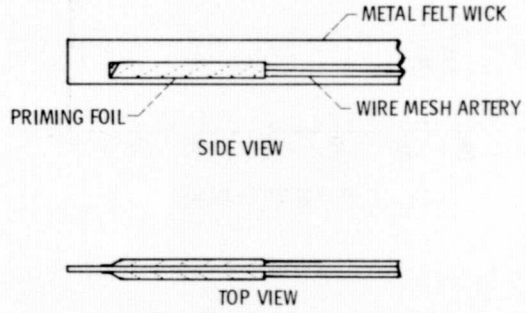

Figure 10. - TEP heat pipe wick assembly.

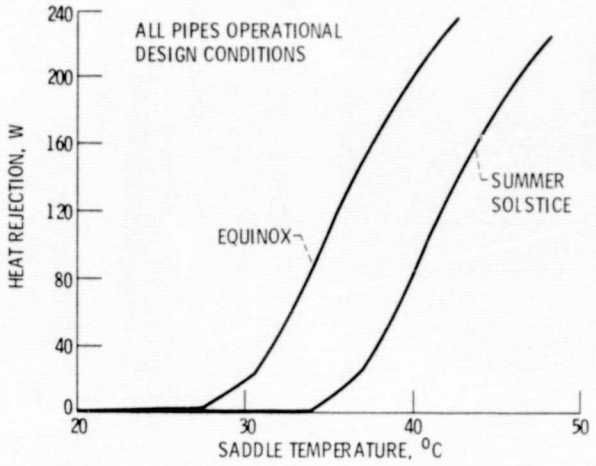

Figure 11. - VCHP system expected performance.

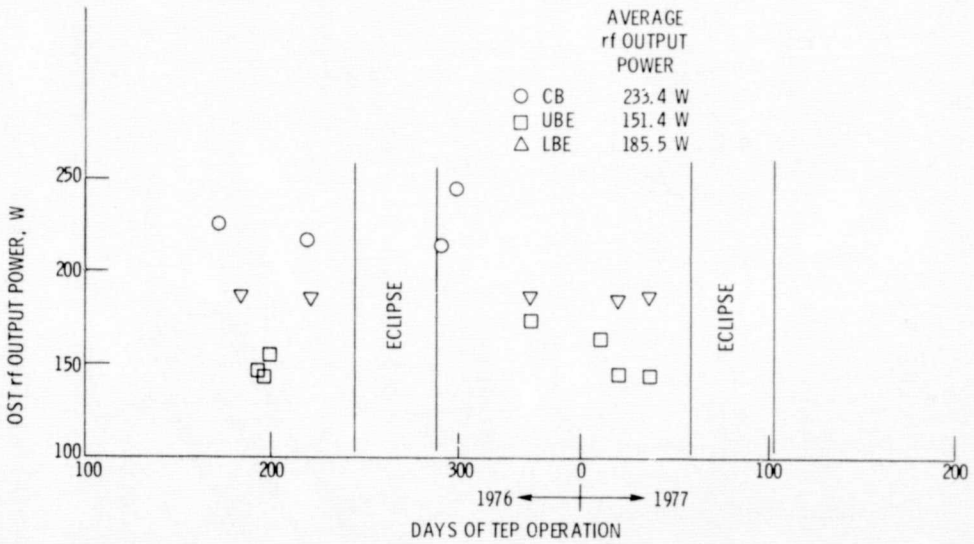

Figure 12. - Hermes OST saturated rf output power at center band, upper band edge, and lower band edge frequencies.

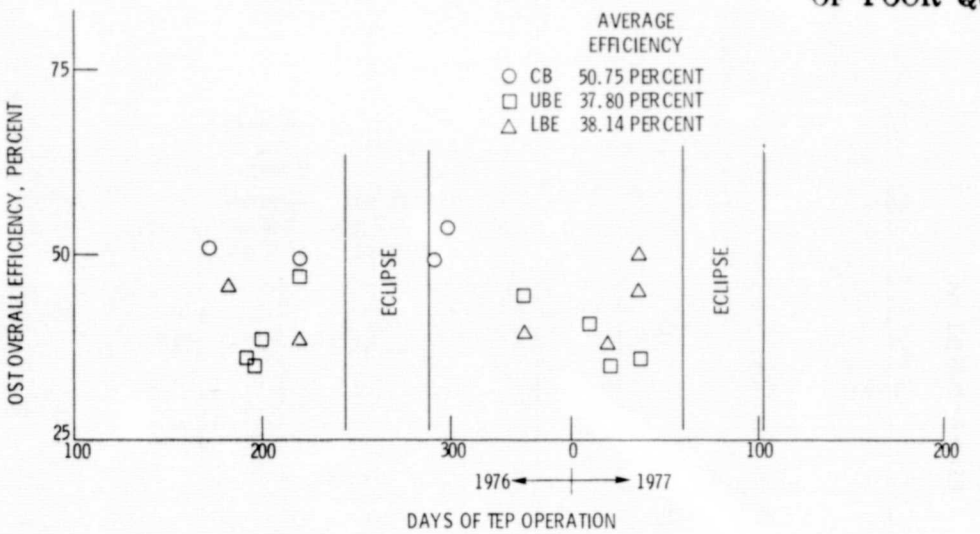

Figure 13. - Hermes OST overall efficiency at saturated rf output power at center band, upper band edge, and lower band edge frequencies.

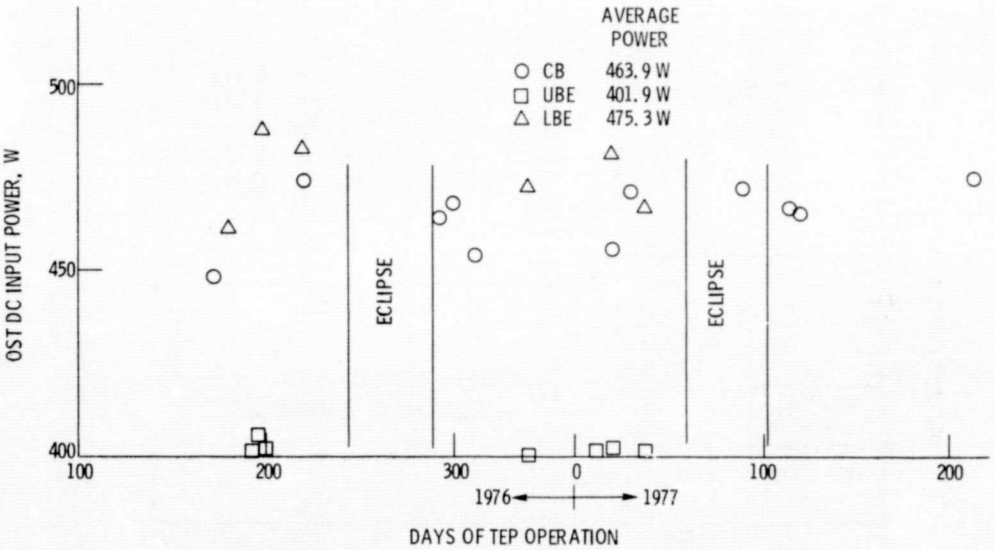

Figure 14. - Hermes OST DC input power for saturated rf output at center band, upper band edge, and lower band edge frequencies.

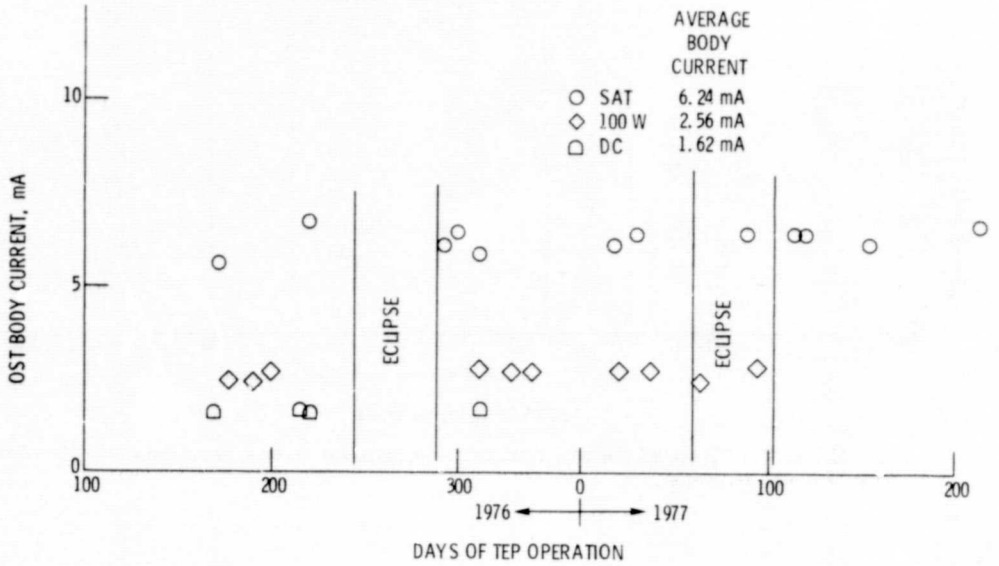

Figure 15. - Hermes OST body current for saturated rf and 100 W rf output at center band frequency and for DC operation.

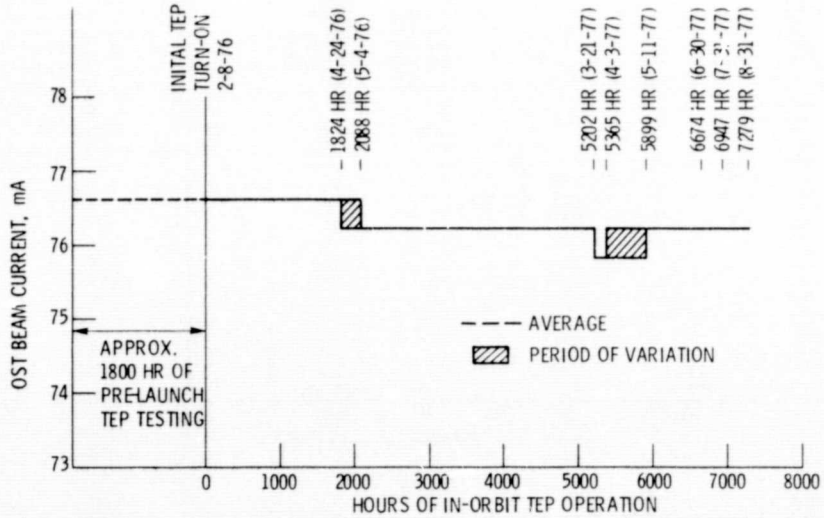

Figure 16. - Hermes OST beam current history to date.

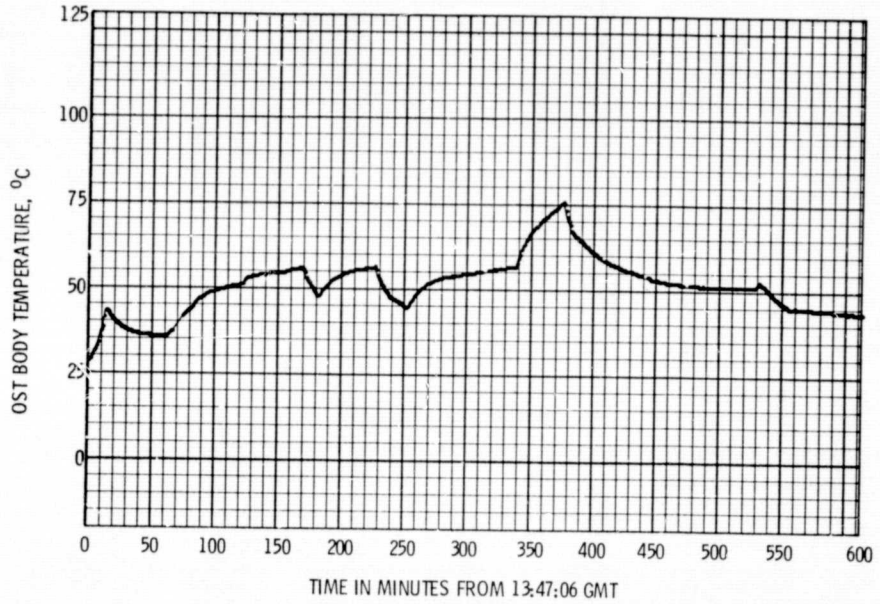

Figure 17. - OST body temperature response to input power changes for day 75.

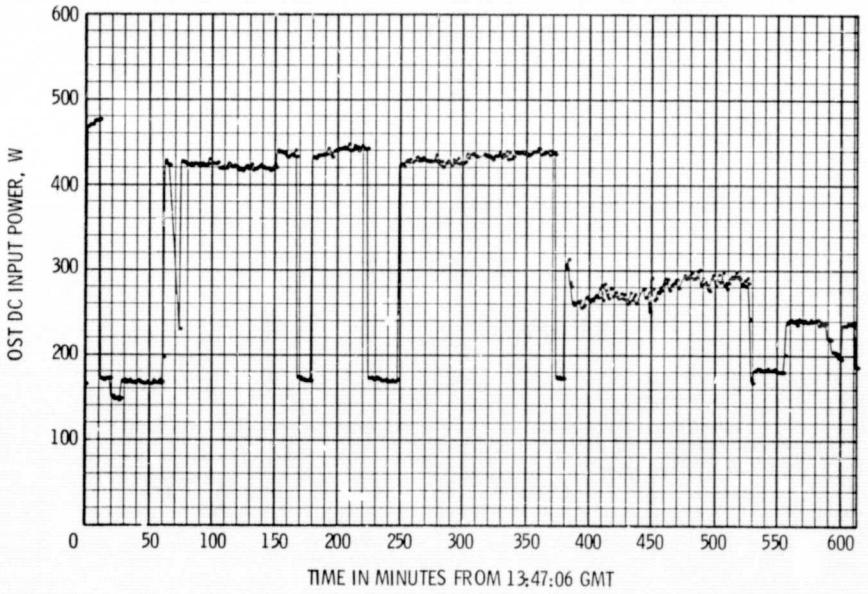

Figure 18. - Electrical input power to OST for day 75.

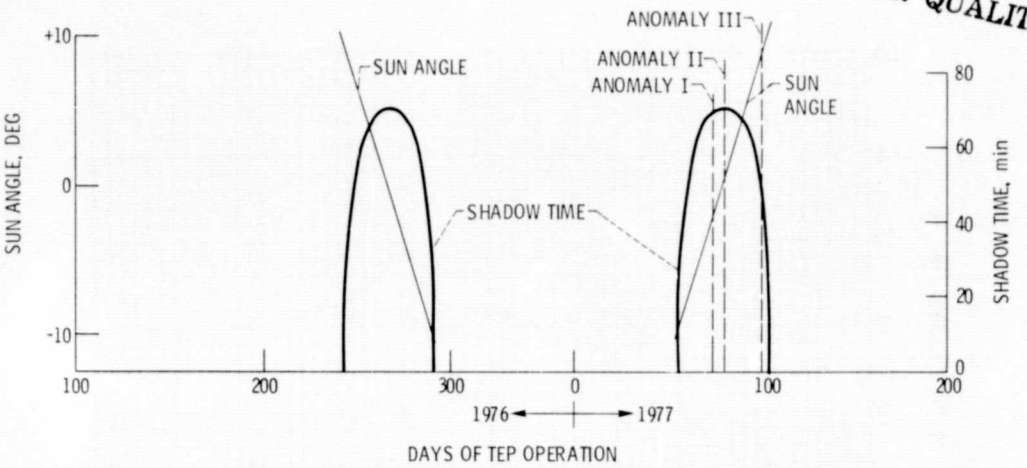

Figure 19. - Eclipse shadow duration and sun angles with respect to spacecraft orbit plane for TEP thermal anomaly days.

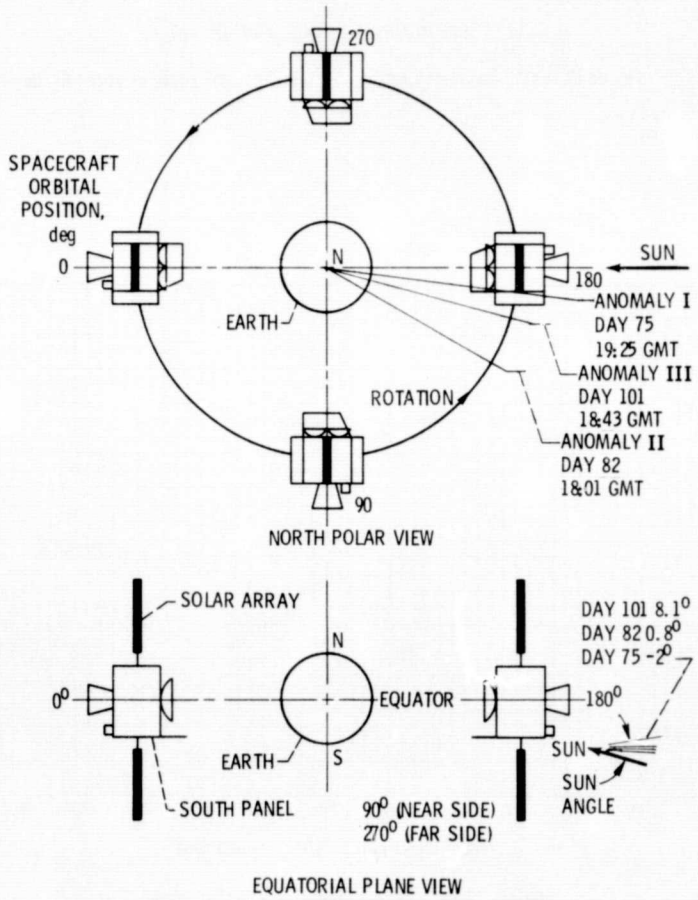

Figure 20. - Hermes spacecraft orbital position and orientation with aspect to Sun illumination for each thermal anomaly day.

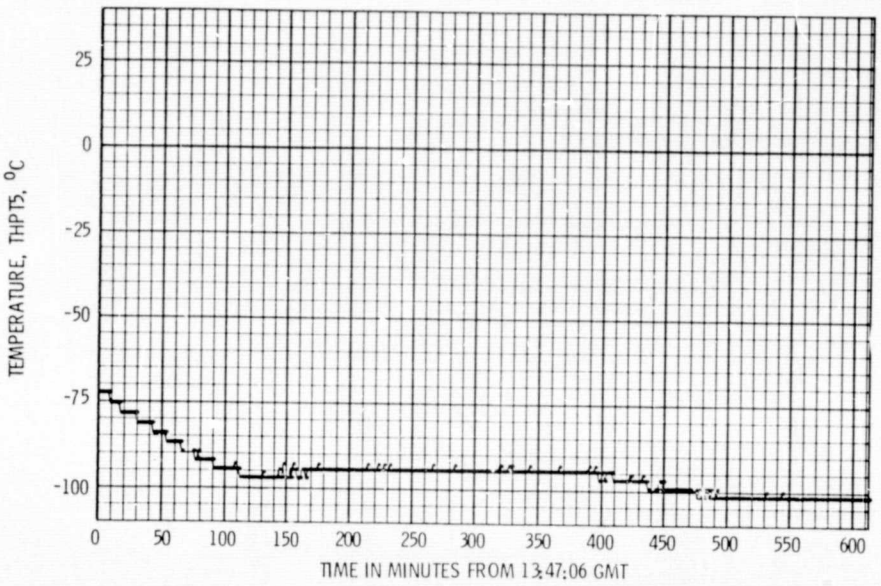

Figure 21. - Heat pipe 1, reservoir-end pipe temperature for day 75.

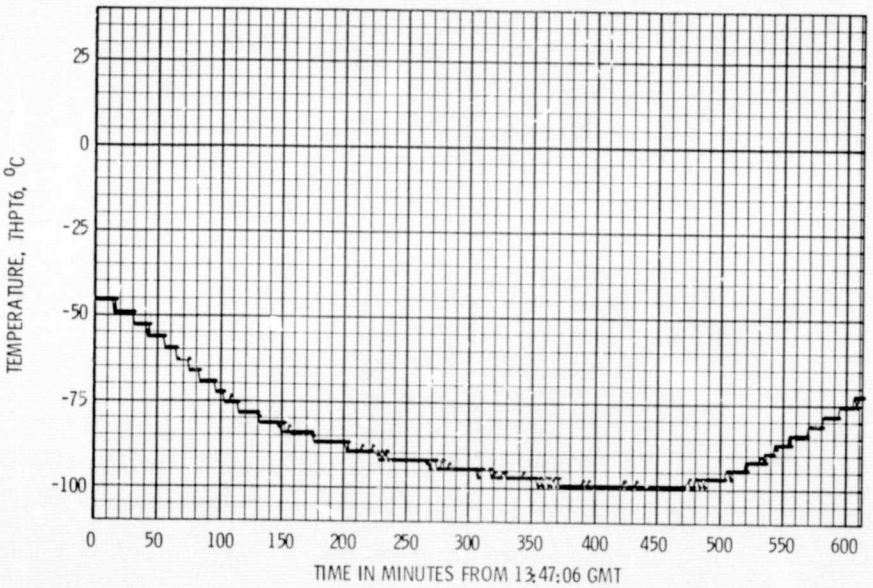

Figure 22. - Heat pipe 1 gas reservoir temperature for day 75.

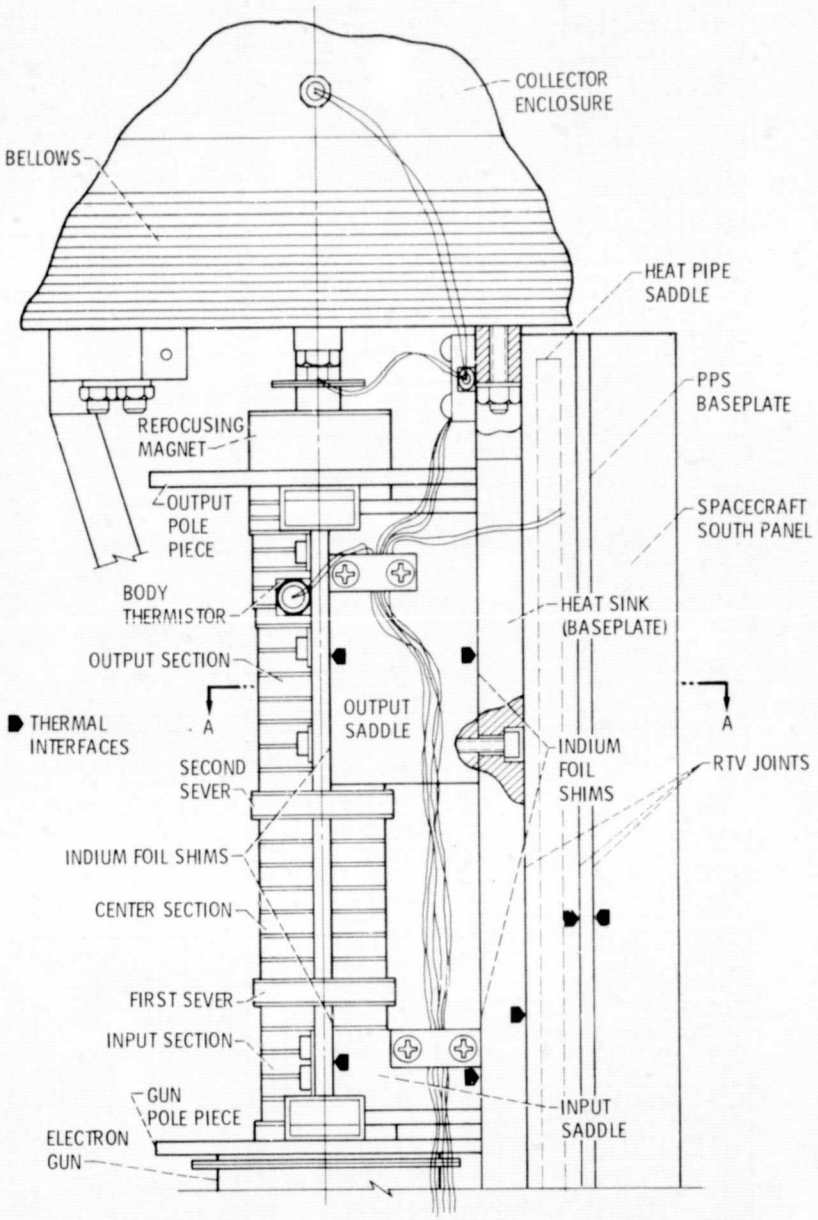

Figure 23. - Mounted CT.

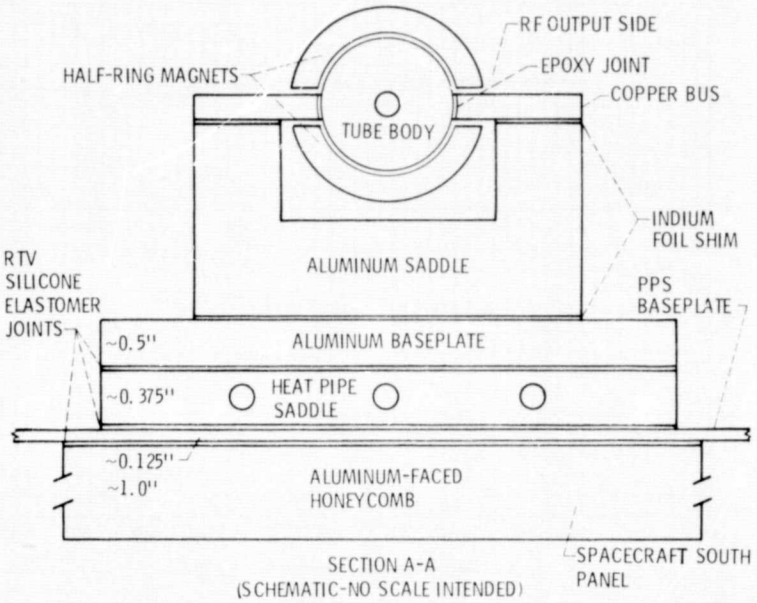

Figure 24. - Thermal conducting mount used for removal of OST body loss heat.

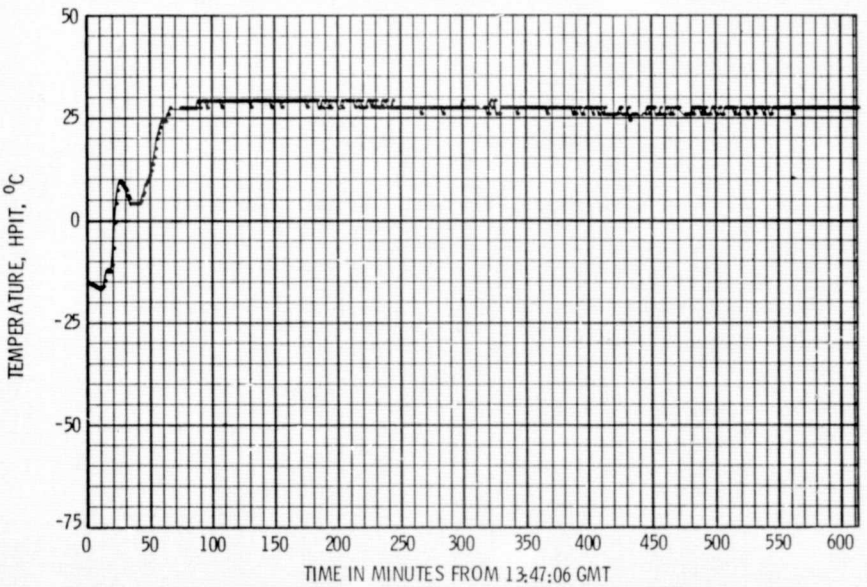

Figure 25. - Heat pipe 1 adiabatic temperature for day 75.

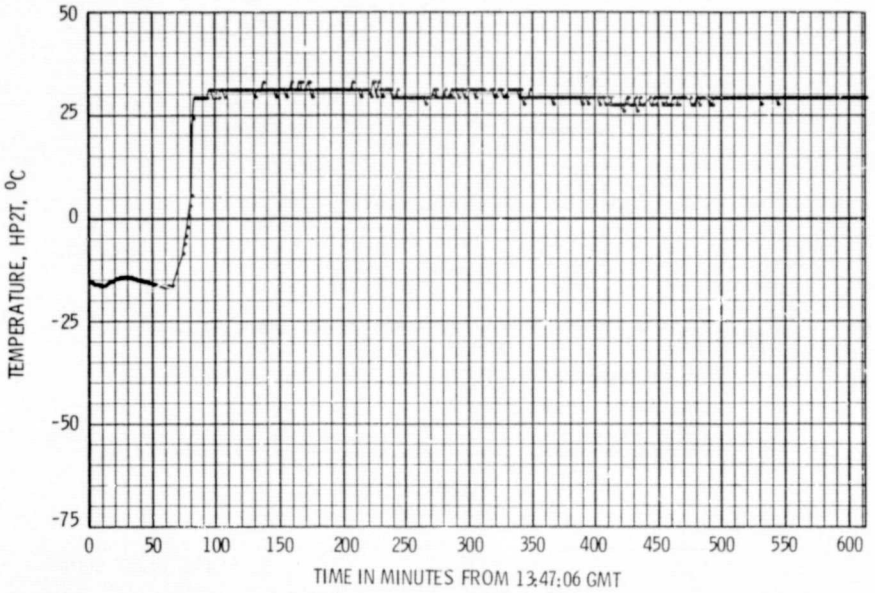

Figure 26. - Heatpipe 2 adiabatic temperature for day 75.

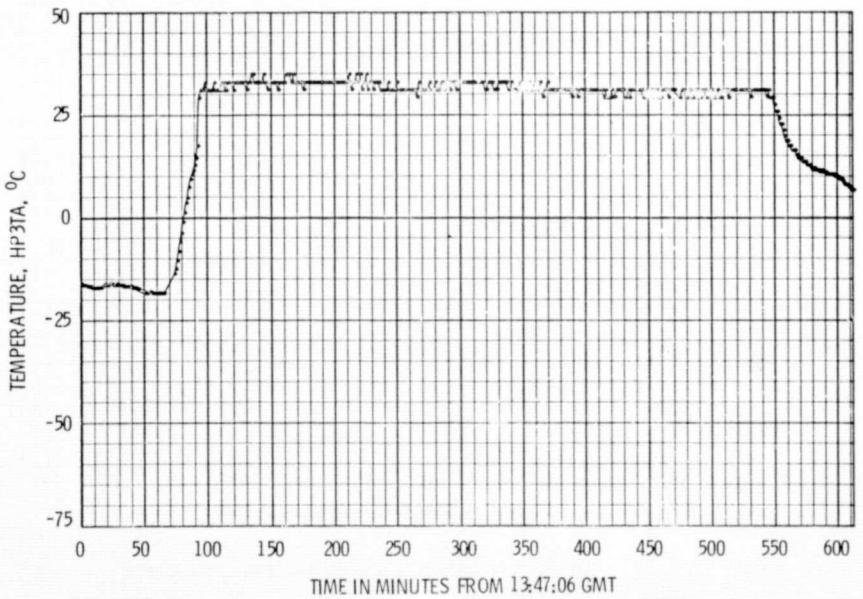

Figure 27. - Heat pipe 3 adiabatic temperature for day 75.

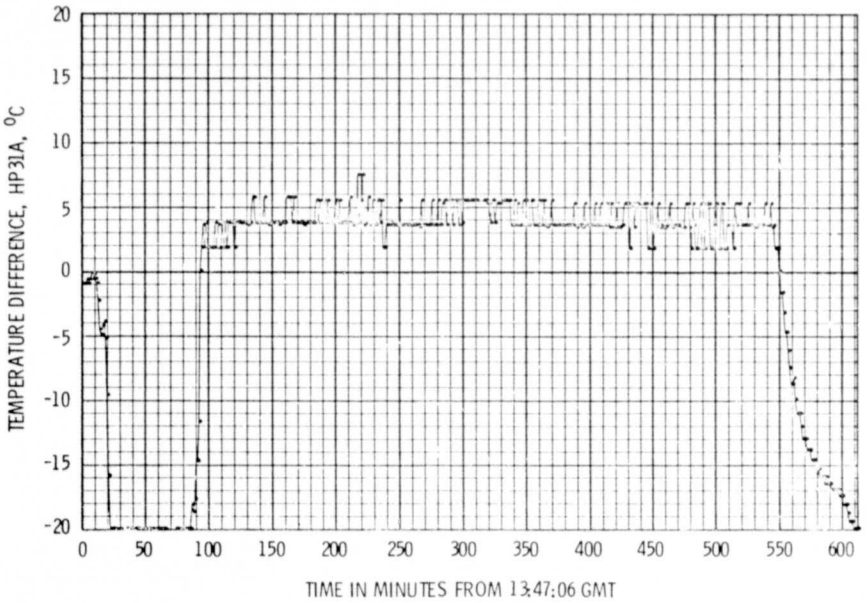

Figure 28. - Difference between heat pipe 3 and heat pipe 1 adiabatic temperatures for day 75.

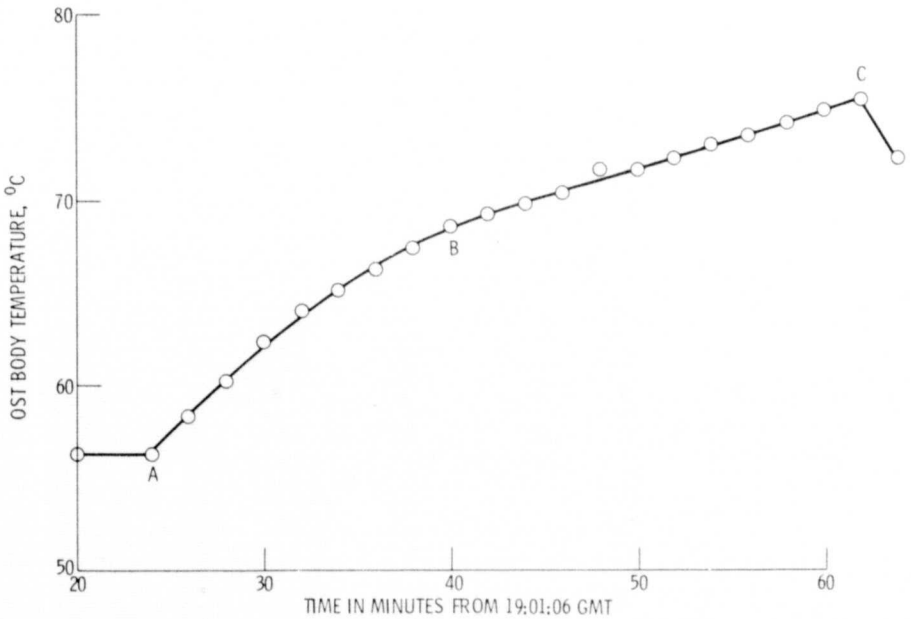

Figure 29. - OST body temperature response during thermal anomaly for day 75.